DISPERSION ANALYSIS OF SPLIT FLEXURAL WAVES

Bertram Nolte, Rama Rao and Xiaojun Huang

June 9, 1997

Abstract

In this paper we first present a technique for measuring dispersion curves from array data, that is both simple and efficient. We demonstrate its performance on both synthetic and field data. We then use the technique to compute dispersion curves for split flexural waves from cross-dipole data from the Powder River Basin in Wyoming. In this data set we consistently observe crossover of the fast and slow flexural waves, an indication of stress-induced anisotropy. Next, we demonstrate the effect that dispersion-curve crossover has on Alford rotation. Finally, we give a procedure for rapidly determining stress-induced anisotropy from crossed-dipole logs.

Introduction

This paper essentially consists of two parts. In the first part we introduce a simple yet efficient technique to measure dispersion curves of guided modes from array data. In the second part we apply this method to study the dispersive behavior of flexural modes for a crossed-dipole data set that was acquired in the Powder River Basin in Wyoming.

In order to estimate phase velocities of dispersive guided waves from array waveforms, a processing scheme is required that will extract the dispersion curves from the data. One commonly used technique to accomplish this task is Prony's method (Lang et al., 1987). A disadvantage of this method is that it often generates spurious estimates (Ellefsen et al., 1993). Another shortcoming is that it requires regularly-spaced receivers, although this is not a problem for data acquired with logging tools with evenly-spaced receivers, such as the Schlumberger Dipole Sonic Imager (DSI). Ellefsen et al. (1993) applied a technique called homomorphic processing and showed that it performed better than Prony's method as it did not generate any spurious arrivals. This method, however, has its own shortcomings. First, it cannot be applied to data in which more than one mode is present at any frequency.

1

Dispersion Analysis

Second, it requires phase unwrapping of the Fourier-transformed data. We will show in this paper that this introduces large errors at frequencies at which the signal amplitudes are low.

Here, we introduce a simple technique that does not suffer from any of the shortcomings of the other two methods. It is not restricted to the presence of only one mode, it does not introduce spurious estimates, it does not require evenly-spaced receivers, and it does not suffer from any problems associated with phase unwrapping.

Part of our motivation to develop this technique was to study the dispersive behavior of flexural waves in anisotropic formations. Flexural waves are dispersive waves that are generated by a dipole source (White, 1967; Kurkjian and Chang, 1986). They exist in both fast and slow formations, and their velocity in the low-frequency limit is the formation shear velocity. One application of the dipole tool is to measure shear velocity in slow formations. Another application is to measure velocities and polarizations of split shear waves in an anisotropic formation. In anisotropic formations the flexural waves generally split into a fast and a slow wave whose polarizations are aligned with those of the fast and slow shear waves propagating parallel to the borehole (Ellefsen et al., 1991; Sinha et al., 1994). The low-frequency velocity limits of these waves are the fast and slow shear velocities, respectively.

Shear velocities are often estimated from dipole-sonic data using a semblance method (Kimball and Marzetta, 1984) followed by a dispersion correction. Other approaches are a model-based inversion (Tang et al., 1995) or a frequency-domain semblance technique (Kimball et al, 1996). In all these applications the flexural-wave dispersion is an undesired effect, and the techniques mentioned above are designed to correct for this effect. However, the dispersive behavior does not necessarily have to be just a nuisance. It can also serve as a source of additional information that would otherwise be unavailable. The work of Winkler et al. (1994), Sinha et al. (1995), and Sinha and Kostek (1996) can be classified in this category. These authors found in both theoretical modeling studies and laboratory experiments that the dispersive behavior of split flexural waves can be an indicator of stress-induced versus intrinsic anisotropy. They found that stress-induced anisotropy causes crossover of the dispersion curves of the two principal components.

In the second part of this paper we use our technique to study the dispersive behavior of split flexural waves from crossed-dipole field data. We will show that these data show the dispersion-curve crossover that is expected for stress-induced anisotropy. We will then describe the effect that dispersion-curve crossover has on four-component data-matrix rotation, generally known as Alford rotation (Alford, 1986), which is the standard technique for rotating data to the principal directions of anisotropy. Finally, we describe a rapid technique for determining whether anisotropy is stress-induced or intrinsic.

2

The Processing Technique

An array tool obtains a measurement of the wavefield at n receivers for each shot. For the DSI tool, $n = 7$ for crossed-dipole measurements and $n = 8$ for monopole measurements. We denote the time-domain data trace on the i-th trace as $d_i(t)$. We start by Fourier transforming the data:

$$d_i(t) \longleftrightarrow D_i(\omega)$$

For each frequency ω we now define a vector $\mathbf{D}(\omega)$:

$$\mathbf{D}(\omega) = \begin{bmatrix} D_1(\omega) \\ D_2(\omega) \\ \vdots \\ D_n(\omega) \end{bmatrix}. \tag{1}$$

The elements of $\mathbf{D}(\omega)$ are the Fourier coefficients of the n receivers at frequency ω. Suppose we have a homogeneous medium in which only one mode is propagating along the z direction. For the frequency (ω) we denote the slowness of this mode by p_z^0 and its attenuation coefficient by a^0. Then the vector components $D_i(\omega)$ and $D_{i+1}(\omega)$ are related by

$$D_{i+1}(\omega) = D_i(\omega) \exp(-a^0 \Delta z) \exp(i\omega p_z^0 \Delta z), \tag{2}$$

where Δz denotes the receiver spacing. The first exponential describes the attenuation, and the second exponential describes the propagation. Here, we do not attempt to measure attenuation, and we will therefore start by describing the processing for velocity only. Later we show that attenuation can be easily incorporated if desired.

We now define a vector $\mathbf{S}(\omega, p_z)$ whose elements are the phase shifts of the receivers relative to the first one:

$$\mathbf{S}(\omega, p_z) = \begin{bmatrix} 1 \\ \exp(i\omega p_z \Delta z) \\ \exp(2i\omega p_z \Delta z) \\ \vdots \\ \exp((n-1)i\omega p_z \Delta z) \end{bmatrix}. \tag{3}$$

Next, we define a fitness function $f(\omega, p_z)$ which is the absolute value of the normalized correlation of the vectors $\mathbf{D}$ and $\mathbf{S}$.

$$f(\omega, p_z) = \frac{|\mathbf{D}^+(\omega)\mathbf{S}(\omega, p_z)|}{\sqrt{\mathbf{D}^+(\omega)\mathbf{D}(\omega)}\sqrt{\mathbf{S}^+(\omega, p_z)\mathbf{S}(\omega, p_z)}}. \tag{4}$$

3

Dispersion Analysis

Here, the superscript + denotes a complex conjugate transpose. The normalization factor $\sqrt{S^+(\omega, p_z)S(\omega, p_z)}$ in the denominator is $\sqrt{n}$ for the vector $S(\omega, p_z)$ of Eq. (3), but will be different if we also want to measure attenuation, as described below.

Due to the normalization, $f(\omega, p_z)$ has a maximum value of 1. By inserting Eqs. (2) and (3) into Eq. (4) it can be seen that this maximum will be attained at $p_z = p_z^0$, i.e. at the true slowness. Maximizing $f(\omega, p_z)$ as a function of p_z for different frequencies will thus give the dispersion curve. In practice, we find that the result can be improved if we proceed in the following way. First we resample our data in the frequency domain (by padding the time-domain traces with zeros). We thus obtain a denser sampling in the frequency domain. We denote the frequency points in this new sampling by (ω_k). Then, instead of maximizing $f(\omega, p_z)$, we maximize

$$F(\omega_k, p_z) = \sum_{j=k-l}^{k+l} W(\omega_j)f(\omega_j, p_z), \tag{5}$$

where $W(\omega_j)$ is a Gaussian weight function:

$$W(\omega_j) = \exp\left(-\frac{(\omega_k - \omega_j)^2}{2\sigma^2}\right). \tag{6}$$

Thus, for each frequency point ω_k the fitness is computed as a weighted fitness average of nearby frequency points ω_j. We maximize $F(\omega, p_z)$ simply by scanning a range of slownesses for each frequency. Some other techniques could be applied for maximizing this function. However, by scanning a slowness range, we can pick up more than one peak of F at each frequency. Even though we have so far assumed that only one mode is present at each frequency, our method can extract more than one mode out of the data, as long as their velocities are not too similar. If more than one mode is present at some frequency then $F(\omega, p_z)$ of Eq. (5) will have a peak for more than one slowness value p_z at that frequency. We illustrate that with an example below. However, if the velocities of two modes are very similar (as is the case for split flexural waves) then the peaks of F (as a function of slowness) may be too wide to separate these two modes. Split flexural waves must therefore be separated in some other way before their dispersion curves can be obtained. Since the modes can be separated by Alford rotation (Alford, 1986; Thomsen, 1988; Esmersoy, 1995), this does not pose a problem, even though care has to be taken in choosing the length of the window over which the Alford rotation angle is estimated, as we demonstrate below.

We will now briefly discuss how the technique has to be modified if one wishes to measure attenuation as well. This amounts to redefining the vector $S(\omega, p_z)$ of Eq. (3) as

4

$$S(\omega, p_z, a) = \begin{bmatrix} 1 \\ \exp((i\omega p_z - a)\Delta z) \\ \exp(2(i\omega p_z - a)\Delta z) \\ \vdots \\ \exp((n-1)(i\omega p_z - a)\Delta z) \end{bmatrix}. \tag{7}$$

We would then maximize f of Eq. 3 of F of Eq. 5 as a function of the two parameters p_z and a. Then, the maximum of f (which is again 1) is attained for $p_z = p_z^0$ and $a = a^0$.

We have given the above equation for the case of evenly-spaced receivers. The method, however is not restricted to this case. If we want to process unevenly-spaced receivers, all we need to do is replace the vector $S(\omega, p_z)$ in Eq. (3) with

$$S(\omega, p_z) = \begin{bmatrix} 1 \\ \exp(i\omega p_z z_2) \\ \exp(i\omega p_z z_3) \\ \vdots \\ \exp(i\omega p_z z_n) \end{bmatrix}, \tag{8}$$

where z_i is the offset from the first receiver to the i-th receiver. Eq. (7) can be modified analogously.

Test With Synthetic Monopole Data

First, we demonstrate our technique on synthetic data. Figure 1 shows an array of eight traces computed for a monopole source. This section was computed for a formation P-slowness of 62.5 μs/ft, a formation S-slowness of 177.6 μs/ft, a borehole fluid slowness of 200 μs/ft, a formation density of 2.6 g/cm^3, a fluid density of 1.0 g/cm^3, and a borehole diameter of 26 cm. The receiver spacing is 0.5 ft. The time sampling interval is 10 μs, and each trace consists of 512 samples. The horizontal units in Figure 1 are the sample numbers. For our processing we resampled this function in the frequency domain by a factor of 4. Our resampled frequency interval is thus 48.8 Hz. We used a Gaussian window in Eq. (5) with a σ of 8 samples and a length l of 3σ.

Figure 2 shows the result of our processing. This figure is a display of the fitness F of Eq. (5) over a range of frequencies and slownesses. The function is displayed in a gray-scale – the lighter the color, the higher the fitness. Also shown are the theoretical dispersion curves of the first two pseudo-Rayleigh modes (Tsang and Rader, 1979; Cheng and Toksöz, 1981) computed for this model. The results from our processing fit these curves reasonably well. In addition to the pseudo-Rayleigh modes our processing also resolved the Stoneley wave, which can be seen in Figure 2 at low frequencies and a slowness slightly higher than that

5

of the borehole fluid. Next, we show the function F at a particular frequency (13 kHz) as a function of slowness only, i.e. we show a cross section of Figure 2 along the white line shown in this figure. This cross section is displayed in Figure 3. It illustrates the width of the peaks of F. As Figure 3 shows, more then one mode can be extracted from the data by our processing, as long as their velocities are not too similar. Here, the two pseudo-Rayleigh modes are well-separated in slowness, and we observe a peak for each of them. However, as mentioned above, the peaks are not narrow enough to resolve modes with very similar velocities, like split flexural waves. We therefore still need to rotate crossed-dipole data to their principal directions, before measuring their dispersion curves.

Figure 4 shows only the peak of the fitness F as a function of frequency and slowness. Again the theoretical dispersion curves are superposed. curves. Even though the peaks of the measured fitness deviate slightly from the theoretical curves, they fit the theoretical curves reasonably well.

Application to Crossed-Dipole Data Analysis

We now apply our technique to the estimation of flexural-mode dispersion curves from crossed-dipole data. The data we use are from ARCO's Red Mountain Well in the Powder River Basin. Wyoming. They were acquired with the DSI tool, which consists of one monopole, two orthogonal dipole sources, and eight pairs of orthogonally-oriented receivers, aligned with the source dipoles. The receiver spacing is 0.5 ft. As the two dipole sources are separated by 0.5 ft, for each source depth there are seven traces, for which the positions of the two sources and of the receivers are the same on both components. Thus seven traces can be used for the array processing. The data consist of 256 samples for each receiver, and the sampling rate is 40 μs. We have logs from two lithological units. the Niobrara formation and the Frontier formation. Both formations are anisotropic and exhibit flexural-wave splitting. However. the anisotropy is significantly higher in the Frontier formation. The Niobrara has some depth regions with very weak anisotropy, which appear almost isotropic (Nolte and Cheng, 1996).

We start by applying our technique to a section recorded in the Niobrara which is fairly isotropic. Figure 5 shows the waveforms recorded on the inline receivers for the lower dipole source. Application of our processing technique produces the result shown in Figure 6. This figure shows the fitness F, displayed in the same way as in Figure 2. For the computation we resampled the frequency by a factor of four. The resampled frequency interval is thus 24.4 Hz. We use a Gaussian window in Eq. (5) with a σ of 8 samples and a length l of 3σ. Note that at higher frequencies the processing appears to be picking up a higher flexural mode. However, since the amplitudes of the signal are very small at these frequencies, this could also be an artifact of the processing. We have not picked up this mode on all the shots we processed. Figure 7 shows the peaks of the fitness together with some theoretical values

(displayed as circles) for a model that was computed for the borehole diameter, formation density, and P-velocity (obtained from the monopole data) for this particular depth section. For the S-velocity we tried different values; the one used to compute the theoretical dispersion in Figure 7 is the one that resulted in the best fit with the measured dispersion. Notice that the higher-order mode agrees reasonably well with the theoretical values, so it could in fact be real and not an artifact of the processing.

Figure 8 shows a comparison of our results with those from homomorphic processing (Ellefsen et al., 1993). This method essentially extracts the dispersion curve by fitting a straight line through the imaginary part of the logarithm of the Fourier transformed spectra as a function of receiver offset. Its main weakness is the need to unwrap the phase of the spectra. As Figure 8 shows, this method performs well at frequencies up to 5 kHz; at higher frequencies, however, severe phase-unwrapping problems occur, so that this method becomes useless. Several points obtained with homomorphic processing are actually outside of the slowness range displayed in this figure.

Analysis of Split Flexural Wave Dispersion

We have shown above that our method produces reasonable results for both synthetic and measured data. We will now use it to analyze in more detail the dispersion characteristics of split flexural waves in the presence of anisotropy. For this purpose we will look at recordings from the Frontier formation, which, as stated above, exhibits significant anisotropy.

A section of waveforms measured in this formation and rotated to the principal anisotropy directions is shown in Figure 9. The fast component is plotted as a solid line, and the slow component as a dashed line. From careful observation of this figure it can be seen that the delay between the two modes decreases with time, and actually reverses its sign at later times, i.e. corresponding peaks of the "slower" mode arrive before those of the "faster" mode. This is already an indication of dispersion-curve crossover.

Before applying our processing technique we will examine the amplitude spectra computed for this shot. Figure 10 shows the spectra on the fast and slow components. For each component it displays the spectra of all seven traces, as well as the mean of these seven spectra. The two figures at the top show the fast component, and the two figures at the bottom show the slow component. First, it can be seen that the amplitude spectra on the seven traces are very consistent at the higher frequencies ($> \sim 3$ kHz) while they are more variable at the lower frequencies. At frequencies $> \sim 6$ kHz the amplitudes get very small on both components. We therefore expect the most accurate results in the frequency range between 3 and 6 kHz. It can be seen that the slow component has smaller amplitudes at the lower frequencies. This is something we observe consistently for all sections in this formation. We do not completely understand the reason for this phenomenon yet, but we have to take it into account when we interpret the results from our processing. As we will see, the

measured dispersion curves for the slower flexural modes will become unreliable at the lower frequencies ($< \sim 2.7$ kHz).

Figure 11 shows the dispersion curves measured with our technique for the fast and the slow components. The most striking feature is the crossover of the two dispersion curves at a frequency of ~ 3.2 kHz. This is essentially the same effect we observed above by examining the time-domain wave forms. As we found, the delay between the two waves not only decreased with time but actually changed sign at later times. We can also see that the slowness of the slower wave decreases with frequency between ~ 2.2 and 2.7 kHz. As we noted above, the amplitudes of this wave are small at these frequencies, and the measurements are therefore not reliable. Above 2.7 kHz, the slower wave shows the expected dispersion behavior.

Interpretation of the Flexural-Wave Crossover

We observe crossover of the two dispersion curves consistently through the entire section recorded in the Frontier formation. We are therefore confident that it is not due to possible inaccuracies of our processing scheme, but that we are measuring a real effect. Recently, it has been shown that dispersion crossover is expected if the anisotropy of the medium is stress-induced (Winkler et al, 1994; Sinha et al., 1995; Sinha and Kostek, 1996). In these studies the authors demonstrate this phenomenon with both theoretical modeling and laboratory experiments. The reason for the crossover is that the borehole itself distorts the stress field. It induces circumferential stresses at the borehole walls, while the radial stresses are zero at the borehole wall. Thus, the stress field at the borehole wall is significantly different from the stress field in the formation. Flexural waves propagating along such a stressed borehole are more sensitive to the stress in the formation at lower frequencies, and more sensitive to the stress in the borehole at higher frequencies.

As our observation is consistent with the studies cited above, we attribute them to stress-induced anisotropy.

Effect of Crossover on Alford Rotation

It is interesting to investigate the implication that dispersion-curve crossover has on Alford rotation, which is the standard technique applied to transform four-component data to the principal directions of anisotropy. As one intuitively expects, the phenomenon of dispersion-curve crossover has the effect that the angle that minimizes the cross-component energies in Alford rotation becomes strongly dependent on the length of the time window over which Alford rotation is applied. The reason for this is that the lower frequencies are associated with higher velocities, thus the shorter the window, the lower the frequencies it will contain. As the flexural-splitting is strongly dependent on frequency (because of crossover, the wave

8

that is faster at low frequencies is slower at high frequencies), rotation of an entire trace by one angle cannot minimize the offline energies at all frequencies. Instead, Alford rotation will minimize the average energy over a range of frequencies, and the angle that does this depends on the length of the rotation window.

We illustrate this with another example from the Red Mountain data set. We pick a section that exhibits a fairly good amount of shear-wave splitting, and also has a fairly symmetric four-component data matrix, as we do not want to complicate our analysis with data-matrix asymmetry problems. Figure 12 shows the four components of this section. The two sections at the top of the figure are the inline components recorded for the upper and the lower source dipole, and the two sections at the bottom show the corresponding offline components. The lines superimposed on the data show the beginning time of the windows over which we will minimize the offline energies.

We now rotate the traces by minimizing the offline energies over windows of different lengths (10, 20, 30, 40, and 50 samples). The rotation angles obtained for these windows are 45°, 40°, 35°, 75°, and 20°, respectively. Figure 13 shows the four components on the first receiver of the original data and of the data rotated to these angles. In each figure the top two traces are the inline components, and the bottom two traces are the offline components. Also shown in each plot is the window over which the rotation is applied. The offline components within each window have the lowest possible offline energy that can be achieved with Alford rotation. Figure 14 shows the flexural-wave dispersion curves computed for the inline components of the original and rotated traces. Unfortunately, as mentioned above, the amplitudes of the slow flexural wave at the low end of the frequency range shown is very small, so that the corresponding dispersion curve is inexact at the lowest frequencies shown in the picture. The slight decrease of slowness with frequency for this wave, from 2.5 Hz to $\sim$ 2.75 kHz, in some of the pictures is an artifact resulting from this problem. To compare the splitting at the low frequency end we therefore need to look at the frequency where the slow flexural wave has its minimum (at $\sim$ 2.75 kHz).

Keeping this in mind we will now compare Figures 14 and 13 to illustrate the point we made above. For a very short window (10 samples) the offline energy vanishes almost completely. The dispersion curves for this case are maximally split at low frequencies. At frequencies roughly between 3 and 3.5 kHz, however, they are hardly split at all. If the window length is increased to 20 samples, the rotation angle changes from 45° to 40°. Figure 13 shows that now the rotation is already unable to eliminate all the offline energy, particularly towards the end of the window. The dispersion curves show that the amount of splitting in the frequency range above 3 kHz has increased over the previous case. At the low frequency end the curves are still well split. Increasing the window length to 30 samples changes the rotation angle to 35°. Rotation to this angle does not change the dispersion curves significantly compared to the 40° rotation. Further increasing the window to 40 samples has a drastic effect both on the time-domain data and on the dispersion curves. Figure 13 shows that when trying to minimize the energy over this window, the early part of the traces remain

9

almost unchanged from the original traces. Figure 14 shows that the dispersion curves do not cross over in the entire frequency range shown. The reason for this is intuitively clear. The rotation tries to maximize the amount of splitting over a large frequency range, which means maximizing the distance of the two dispersion curves over a large range, hence no crossover. Further increasing the window length to 50 samples changes the rotation angle to 20°. Figure 13 shows that now the energy has been reduced mainly in the later part of the window at the expense of the earlier part. The corresponding dispersion curves show that the splitting at the highest frequencies has increased over the previous case. At the low frequency end there is now splitting again.

These observations suggest that particular care has to be taken when rotating flexural wave forms. The window should be as short as possible (but long enough to still obtain consistent rotation angles), since only then will the traces be rotated approximately to the principal directions of the formation. For longer windows the distorted stress in the borehole will cause the rotation angle to be wrong.

A Rapid Technique for Measuring Stress-Induced Anisotropy

Sinha and Kostek (1996) suggest that, since dispersion-curve crossover only happens for stress-induced anisotropy, it can be used as an indicator for stress-induced anisotropy. Our technique suggests a rapid way of measuring this indicator over a range of depths. We suggest proceeding as follows. First, perform the Alford rotation using a short window. Then, find out which mode is slow and which is fast by means of a correlation of the rotated waveforms over the length of the rotation window. Next, compute the dispersion curves for the two flexural waves for a few frequencies only, which should be in the range where the curves have already crossed over (between 4 and 4.5 kHz would be a good choice for the data set we presented here), and determine which mode is faster. Comparing these two measurements will then determine if the curves cross over. Computing the dispersion curves for only a small frequency range will cut down the (already small) computation time, and will speed up the method enough that it can be used as a routine procedure for large data sets.

Conclusions

We have presented a simple technique that performs dispersion analysis accurately and fast. We have demonstrated that it works well both on synthetics, and on field data, even if more than one mode is present. We applied it to a crossed-dipole dataset. Here, we consistently observed crossover of the dispersion curves of the fast and slow flexural waves. We viewed this as an indication of stress-induced anisotropy, which is consistent with laboratory experiments and theoretical predictions. We finally suggested a rapid technique for the detection of stress-induced anisotropy.

Acknowledgments

REFERENCES

Alford, R. M., 1986, Shear data in the presence of azimuthal anisotropy, *56th Ann. Int. Mtg. Soc. Expl. Geophys., Expanded Abstracts*, 476–479.

Cheng, C .H. and Toksöz, M. N., 1981, Elastic wave propagation in a fluid-filled borehole and synthetic acoustic logs, *Geophysics, 46*, 1042–1053.

Ellefsen, K. J., Burns, D. R., and Cheng, C. H., 1993, Homomorphic processing of the tube wave generated during acoustic logging, *Geophysics, 58*, 1400–1407.

Ellefsen, K. J., Cheng, C. H., and Toksöz M. N., 1991, Applications of perturbation theory to acoustic logging, *J. Geophys. Res., 96*, 537–549.

Esmersoy, C., 1995, Dipole shear anisotropy logging, *64th Ann. Int. Mtg. Soc. Expl. Geophys., Expanded Abstracts*, 1139–1142.

Kimball, C. V. and Marzetta, T. L., 1984, Semblance processing of borehole acoustic array data, *Geophysics, 49*, 274–281.

Kimball, C. V., Scheibner, D. J., and Saiki, Y., 1996, Dispersive wave processing of the borehole flexural mode, *66th Ann. Int. Mtg. Soc. Expl. Geophys., Expanded Abstracts*, 170–173.

Kurkjian, A. L. and Chang, S. K., 1986, Acoustic multipole sources in fluid filled boreholes, *Geophysics, 50*, 852-866.

Lang, S. W., Kurkjian, A. L., McClellan, J. H., Morris, C. F., and Parks, T. W., 1987, Estimating slowness dispersion from arrays of sonic logging data, *Geophysics, 52*, 530–544.

Nolte, B., and Cheng, C. H., 1996., Estimation of nonorthogonal shear-wave polarizations and shear-wave velocities from four-component dipole logs, *Borehole Acoustics and Logging and Reservoir Delineation Consortia, Annual Report, Earth Resources Laboratory, M.I.T.* 2-1-2-20.

Sinha, B. K., Norris, A. N., and Chang, S. K., 1994, Borehole flexural modes in anisotropic formations, *Geophysics, 59*, 1037–1052.

Sinha, B. K., Plona, T. J., Winkler, K. W., and D'Angelo, R. M., 1995, Stress-induced dipole anisotropy in a dry Berea sandstone, *65th Ann. Int. Mtg. Soc. Expl. Geophys., Expanded Abstracts*, 22–25.

Sinha, B. K. and Kostek, S., 1996, Stress-induced anisotropy in borehole flexural waves, *Geophysics, 61*, 1899–1907.

Tang, X. M., Reiter, E. C., and Burns, D. R., 1995, A dispersive-wave processing technique for estimating formation shear velocity from dipole and Stoneley waveforms. *Geophysics, 60*, 19–28.

Thomsen, L., 1988, Reflection seismology over azimuthally anisotropic anisotropic media. *Geophysics, 53*, 304–313.

Tsang, L. and Rader, D., 1979, Numerical evaluation of the transient acoustic waveform due to a point source in a fluid-filled borehole, *Geophysics, 44*, 1706–1720.

Dispersion Analysis

White, J. E., 1967, The hula log – a proposed acoustic tool, *Trans. Soc. Well Log Anal. 8th Ann. Sympos.*, paper 1.

Winkler, K. W., Plona, T., Hsu, C.-J., Sinha, B. K., and Kostek, S., 1994, Effects of borehole stress concentrations on dipole anisotropy measurements, *64th Ann. Int. Mtg. Soc. Expl. Geophys., Expanded Abstracts*, 1136–1138.
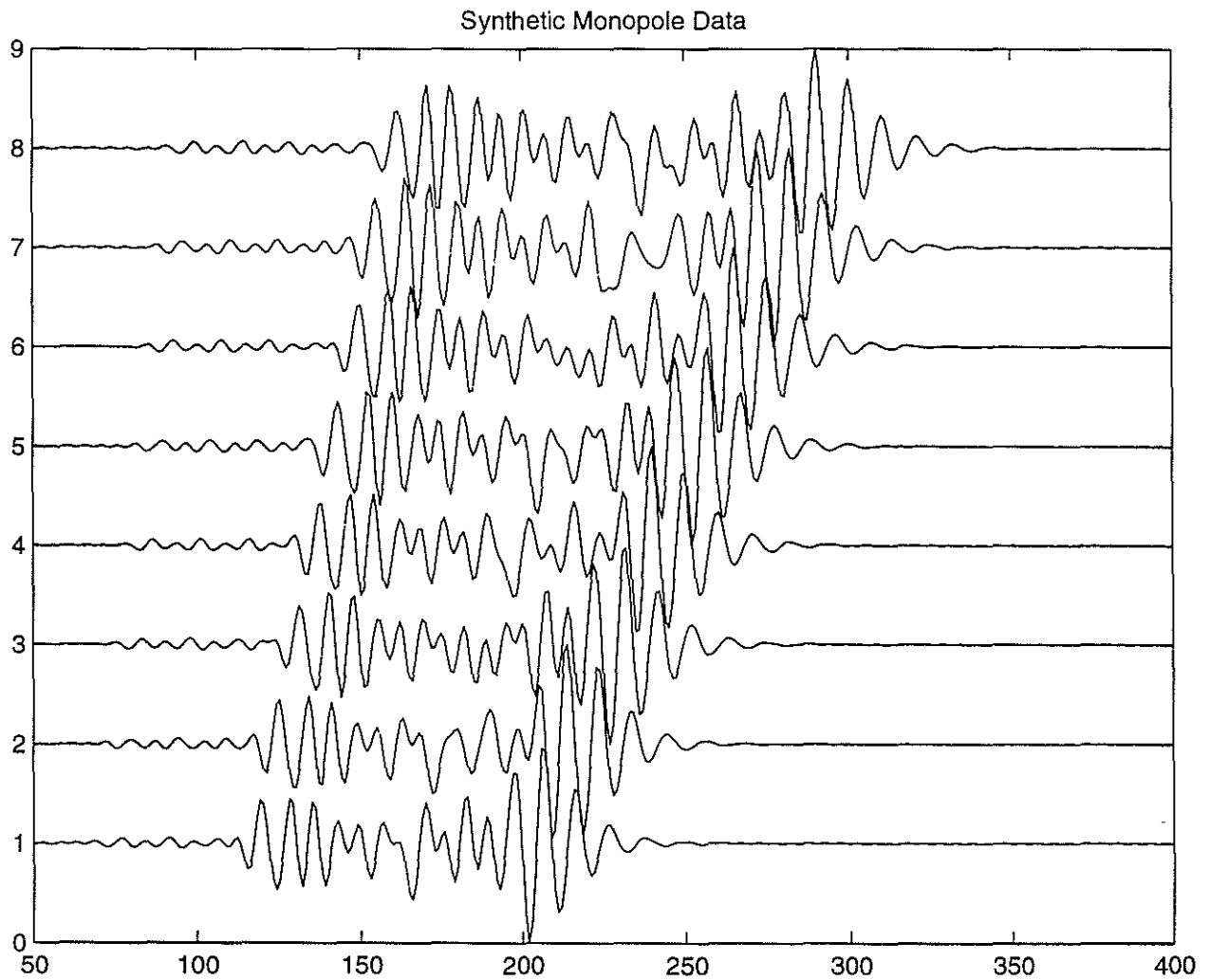
Synthetic Monopole Data

Figure 1: Synthetic monopole data used to test our processing technique. The unit on the x-axis is the sample number. The sampling interval is 10 μs. The parameters used for the computation are given in the text.
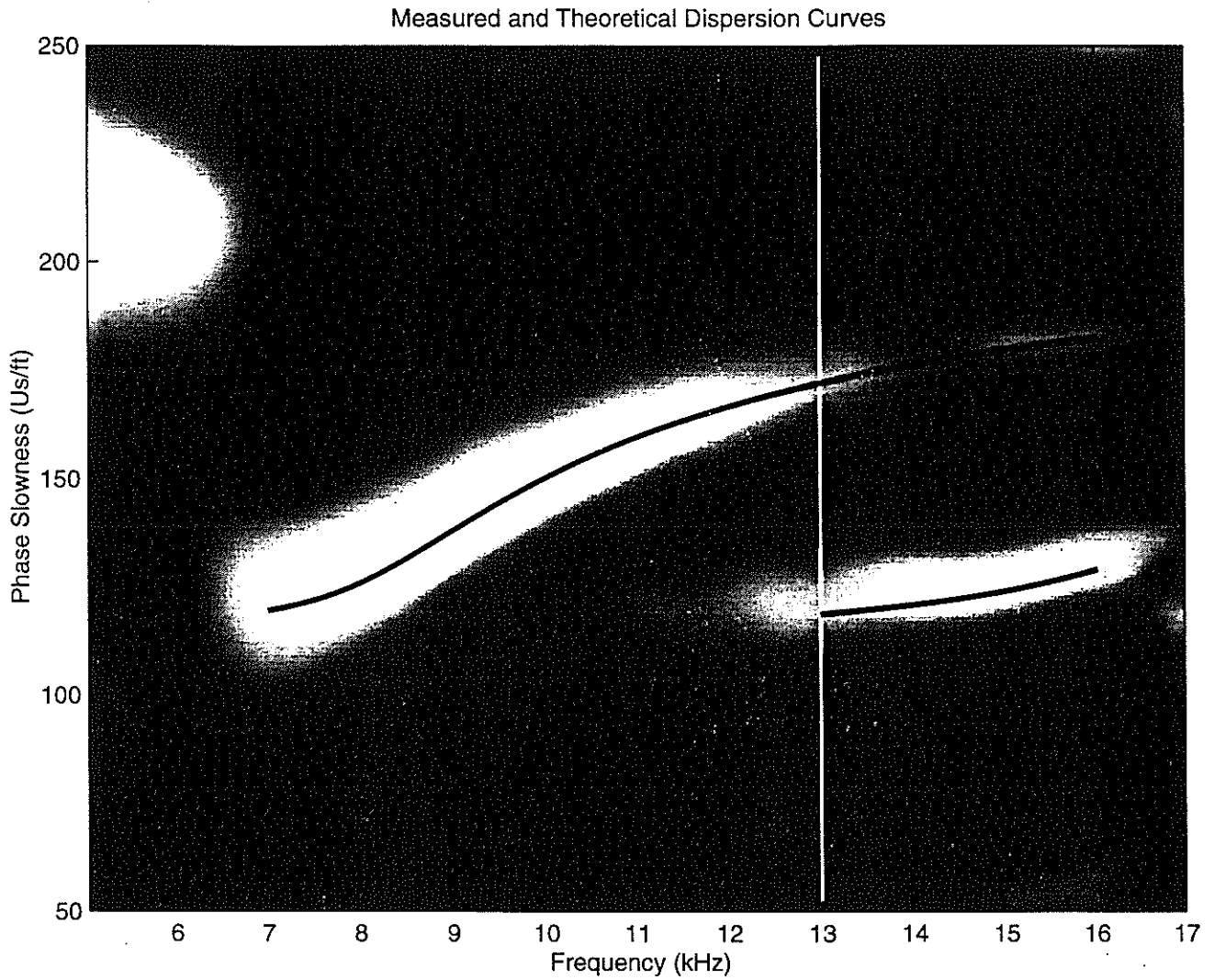
Figure 2: Fitness as a function of frequency and slowness, computed with our method, displayed on a gray scale. Lighter colors indicate higher fitness, darker colors indicate lower fitness. The black curves are theoretical dispersion curves for pseudo-Rayleigh modes. The white line indicates the position of the profile displayed in Figure 3.

Measured Fitness at 13 kHz
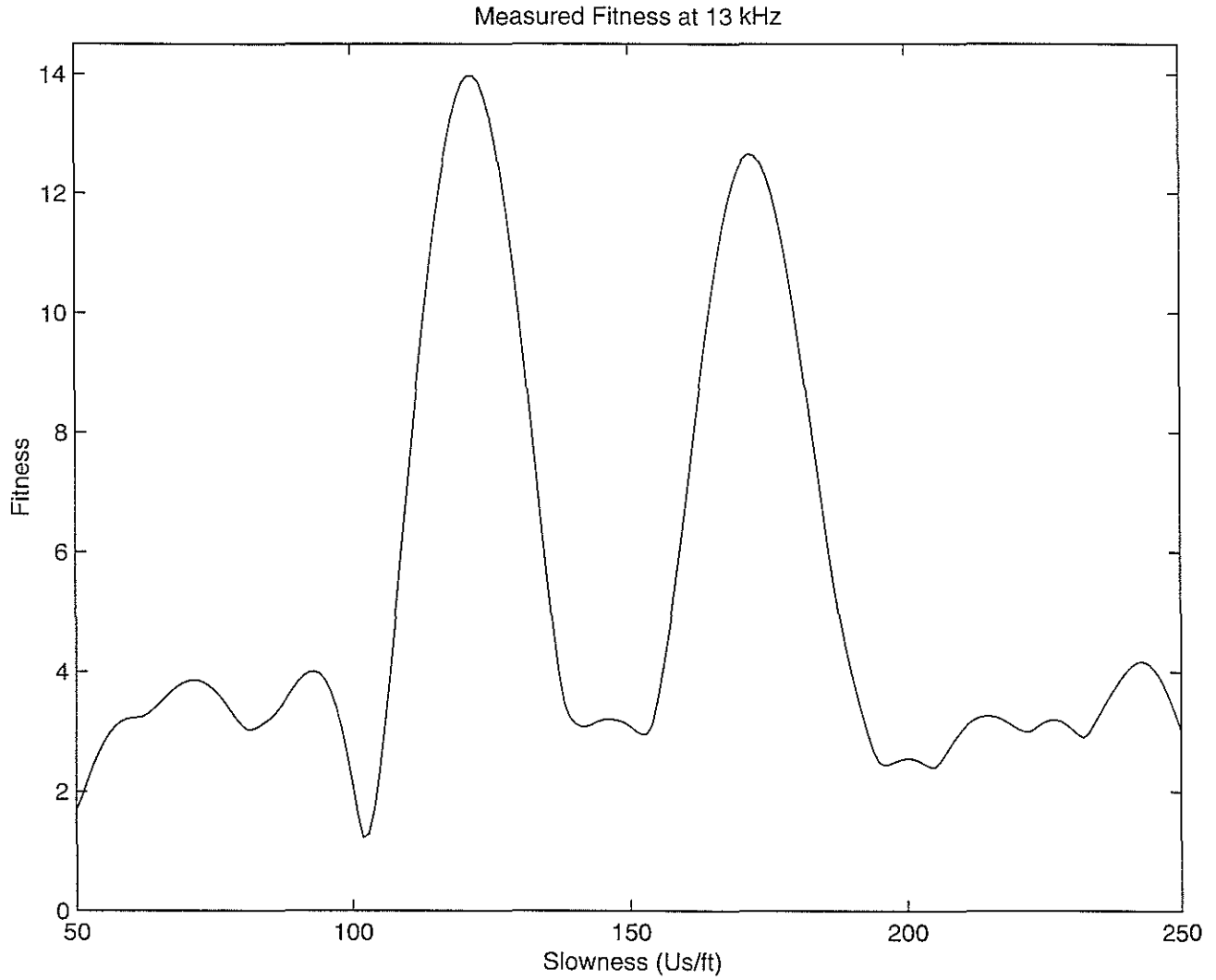
Figure 3: Fitness as a function of slowness at 13 kHz. The two peaks correspond to the two pseudo-Rayleigh modes present at this frequency.
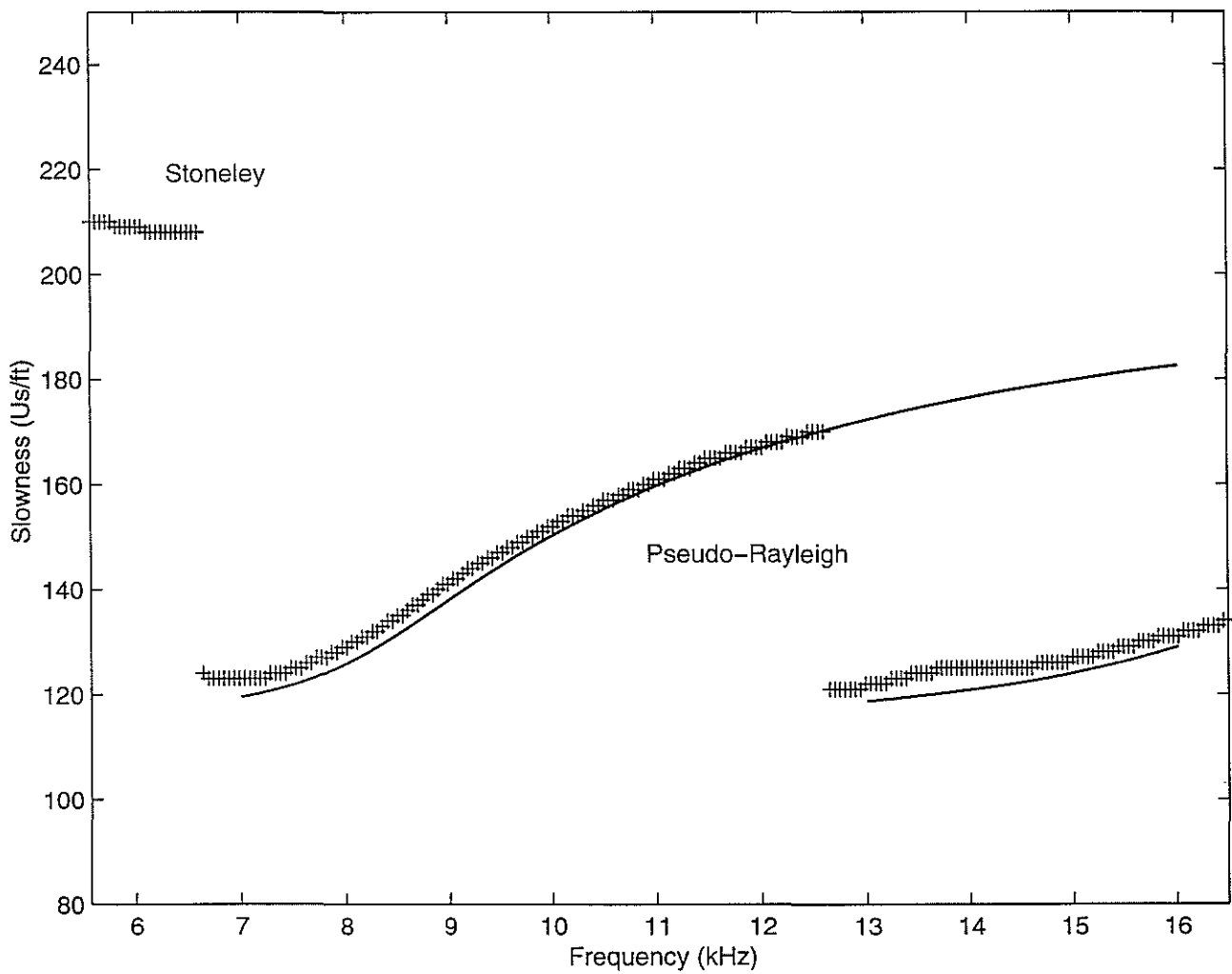
Figure 4: Peaks of the fitness displayed in Figure 2 and theoretical dispersion curves of the pseudo-Rayleigh modes.
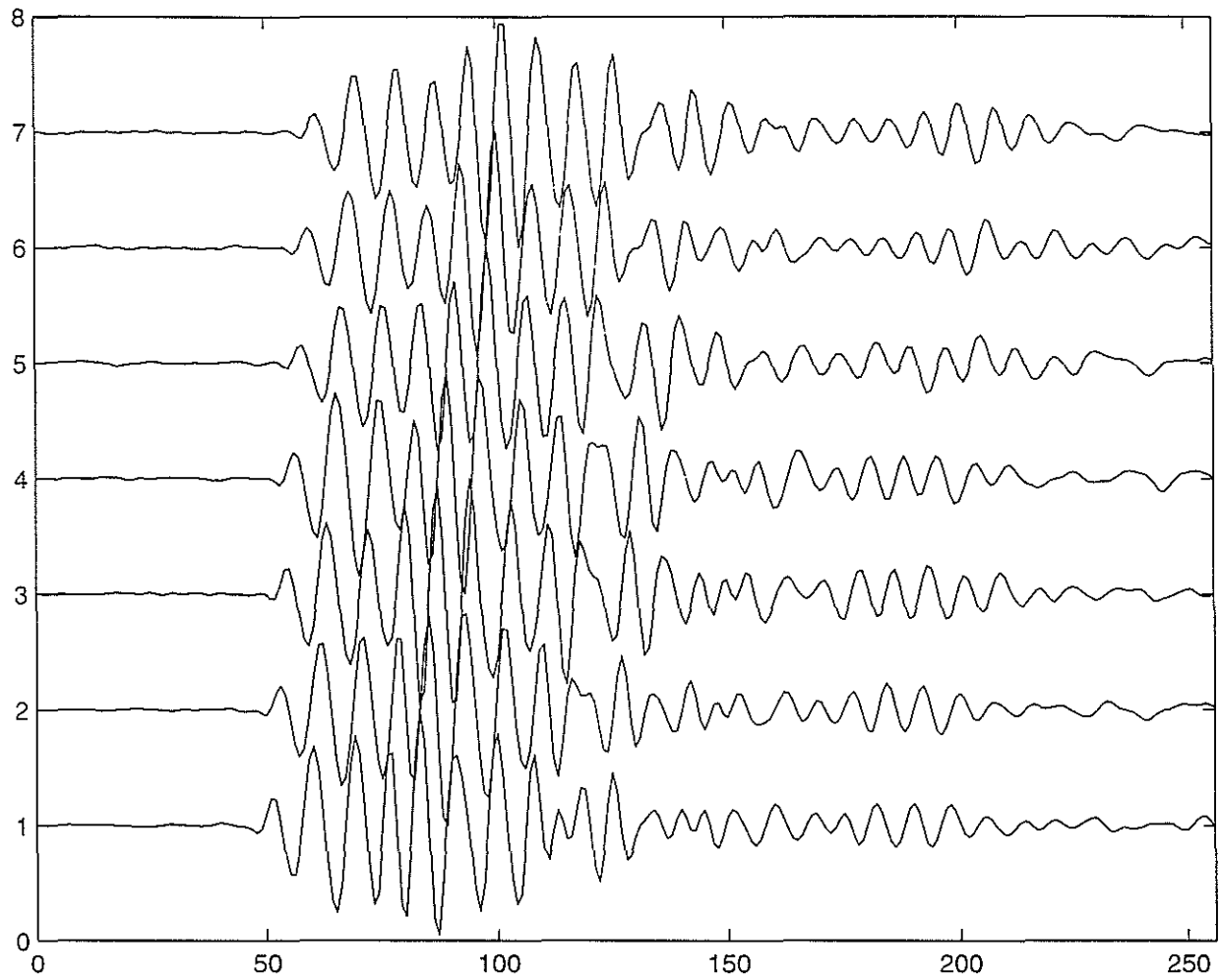
Figure 5: Dipole waveforms measured with the DSI in the Niobrara formation. These waveforms correspond to an inline component at a depth that exhibits only a very small amount of anisotropy.
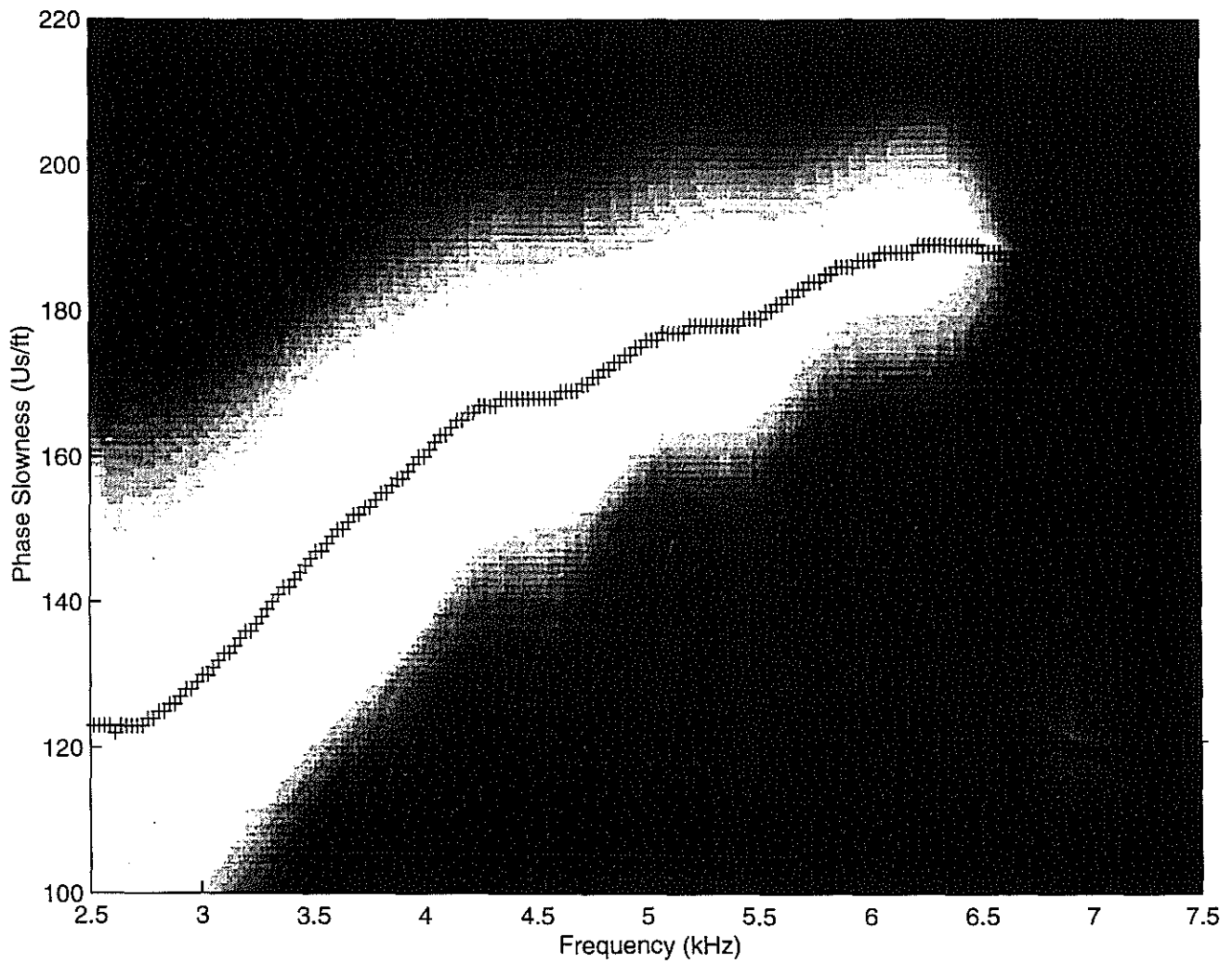
Figure 6: Result of our processing applied to the data in Figure 5. The display is as in Figure 2. The peak of the fitness is also shown.
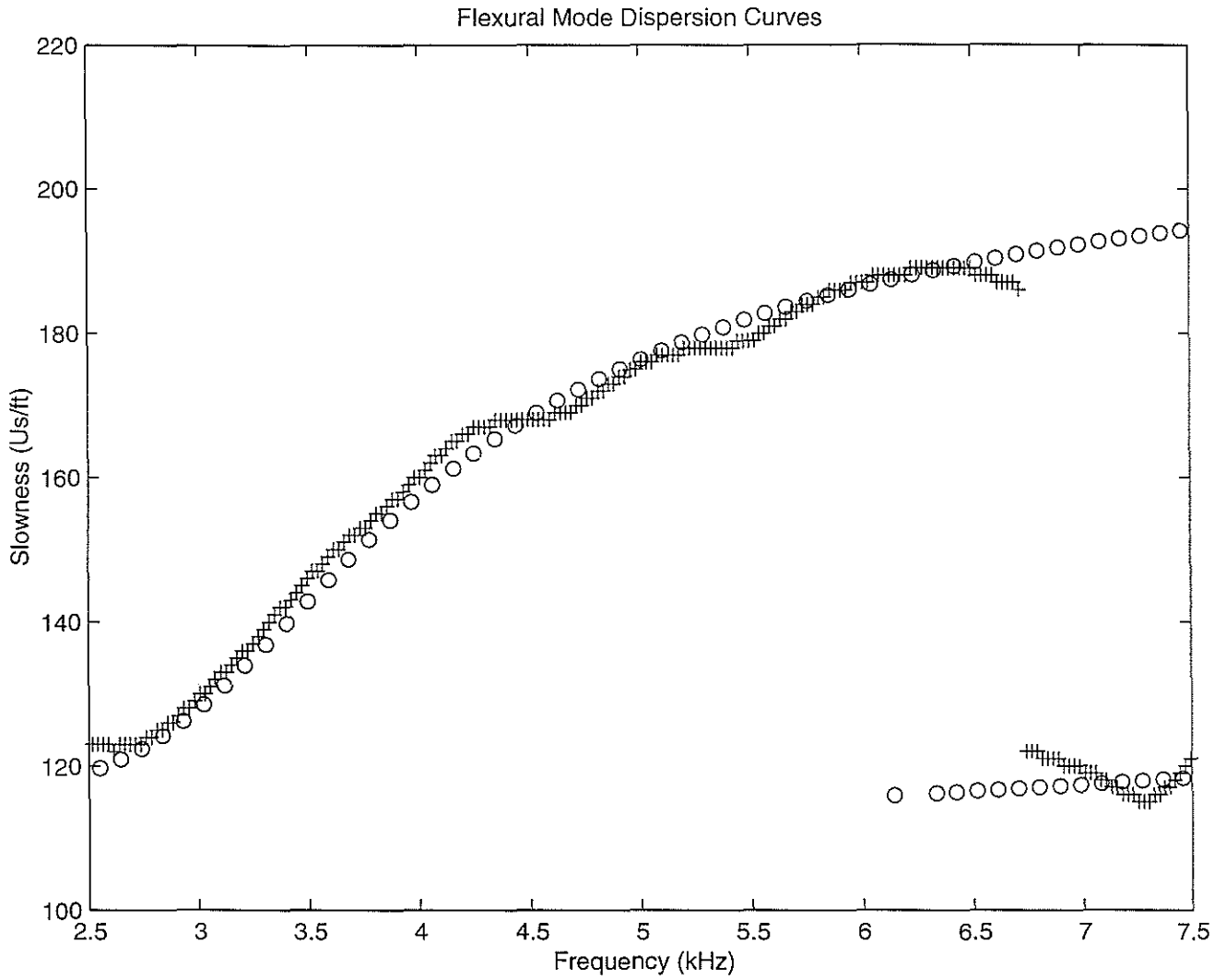
Figure 7: The peak of the fitness of Figure 6 (crosses) computed from the data in Figure 5 and theoretical dispersion curves (circles) of flexural modes.

–
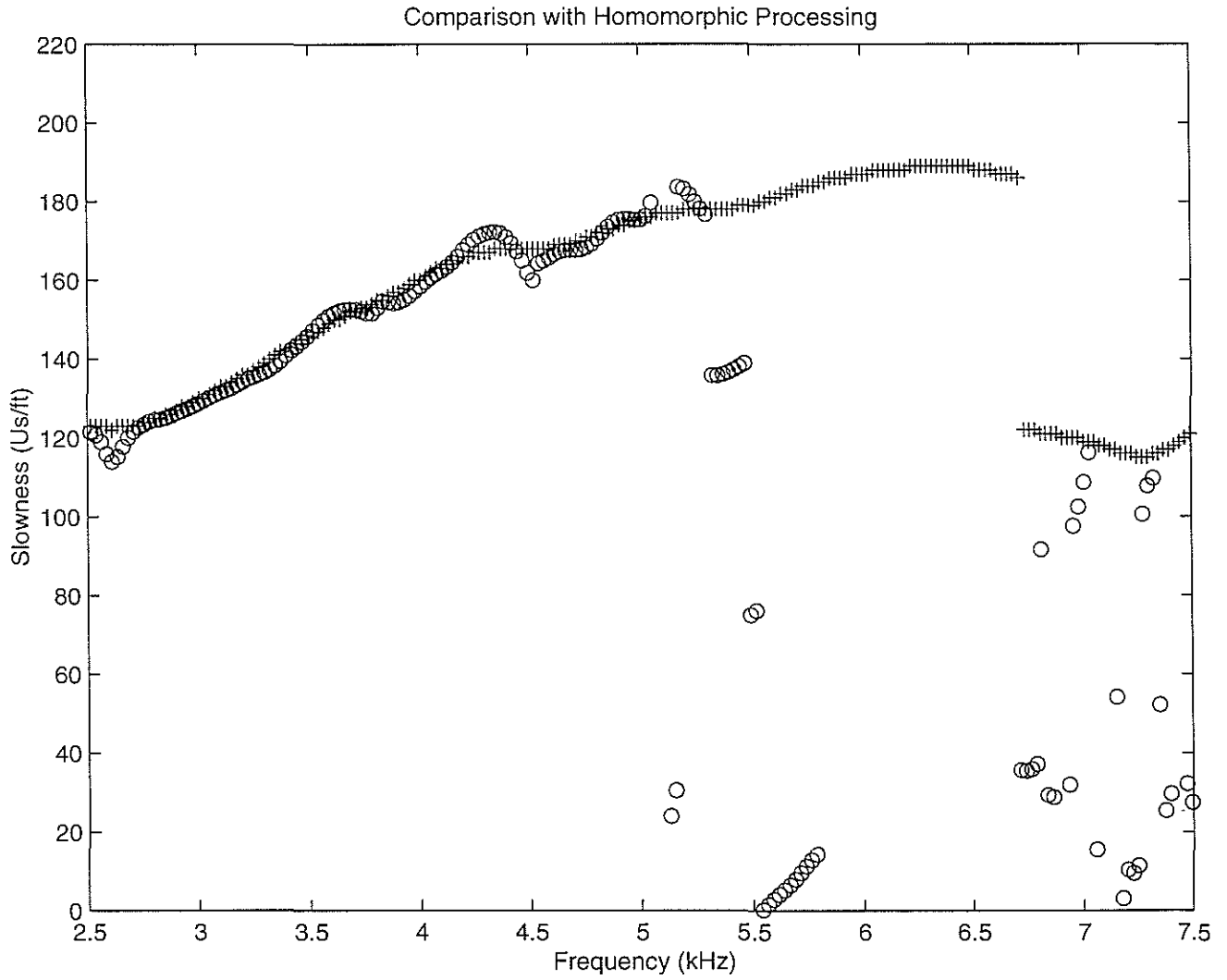
Figure 8: The peak of the fitness of Figure 6 (crosses) and results from homomorphic processing (circles).
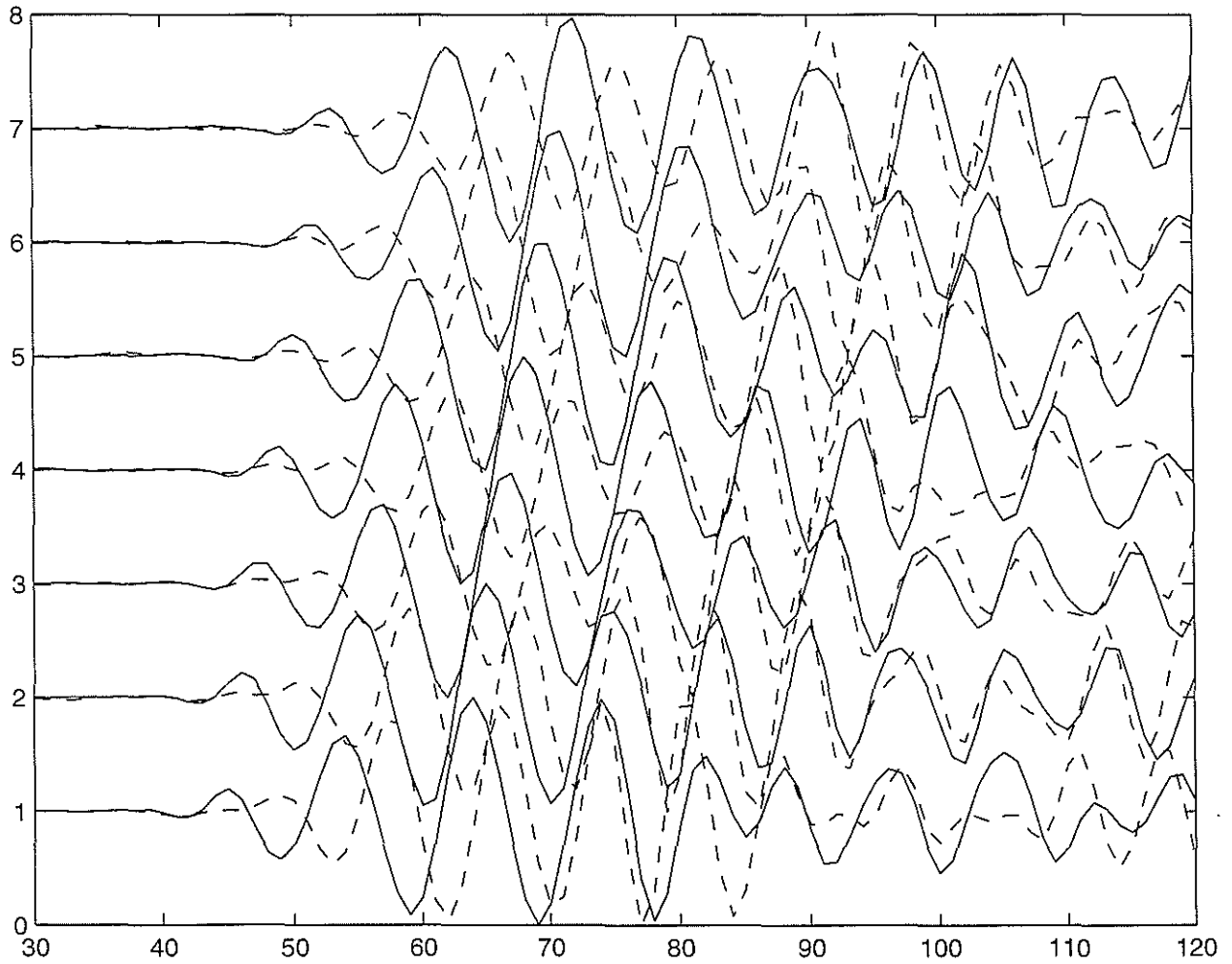
Figure 9: Flexural waveforms on the fast (solid lines) and slow (dashed lines) components for a strongly anisotropic section of the Frontier formation.
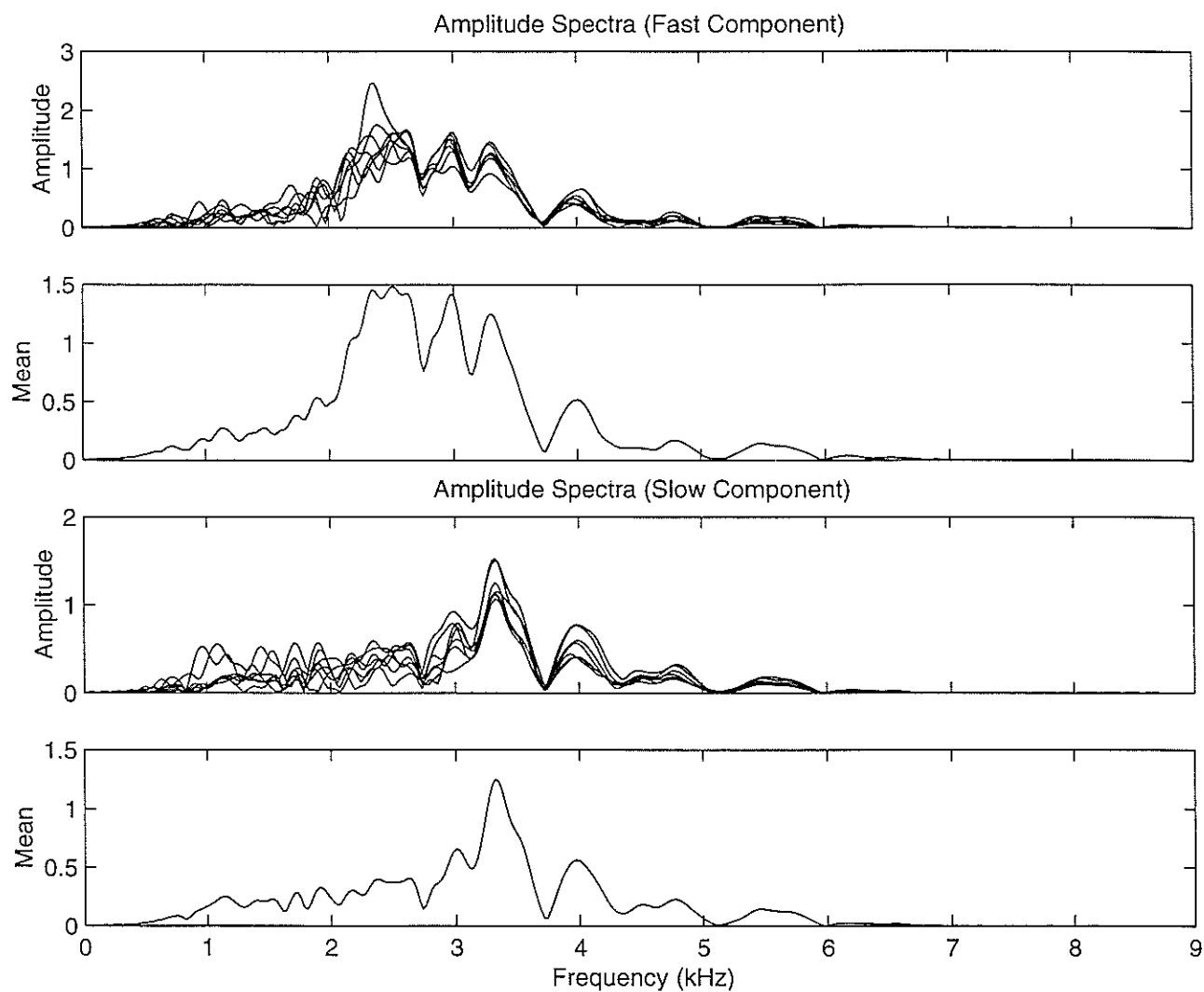
Figure 10: Amplitude spectra of the fast (top 2 pictures) and slow (bottom 2 pictures) traces of Figure 9. For each component the upper picture shows the spectra on all 7 traces while the lower picture shows the average spectrum of the 7 traces.

23

Dispersion Analysis
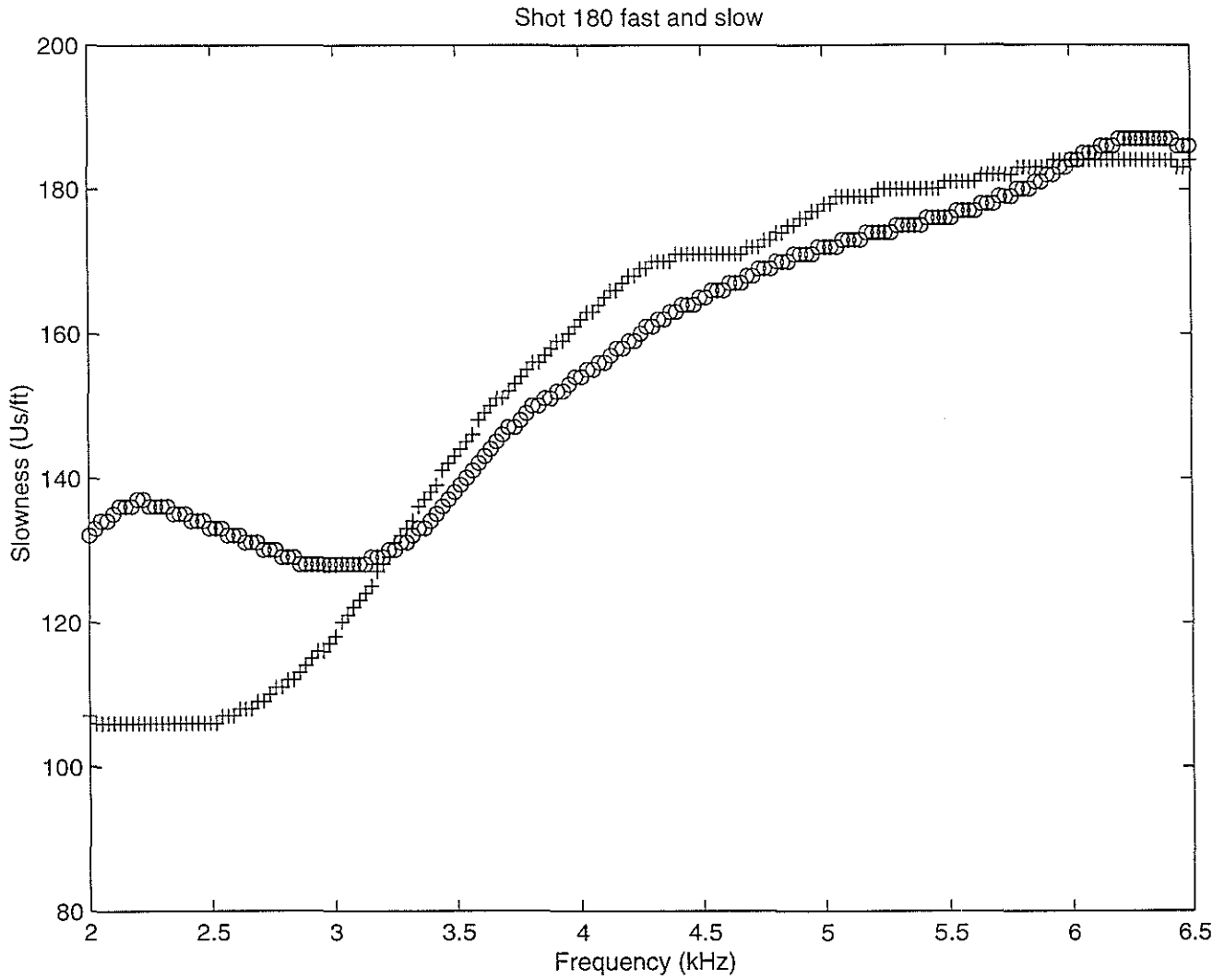
Figure 11: Flexural dispersion curves obtained from the data in Figure 9 with our processing technique for the fast (crosses) and the slow (circles) component.
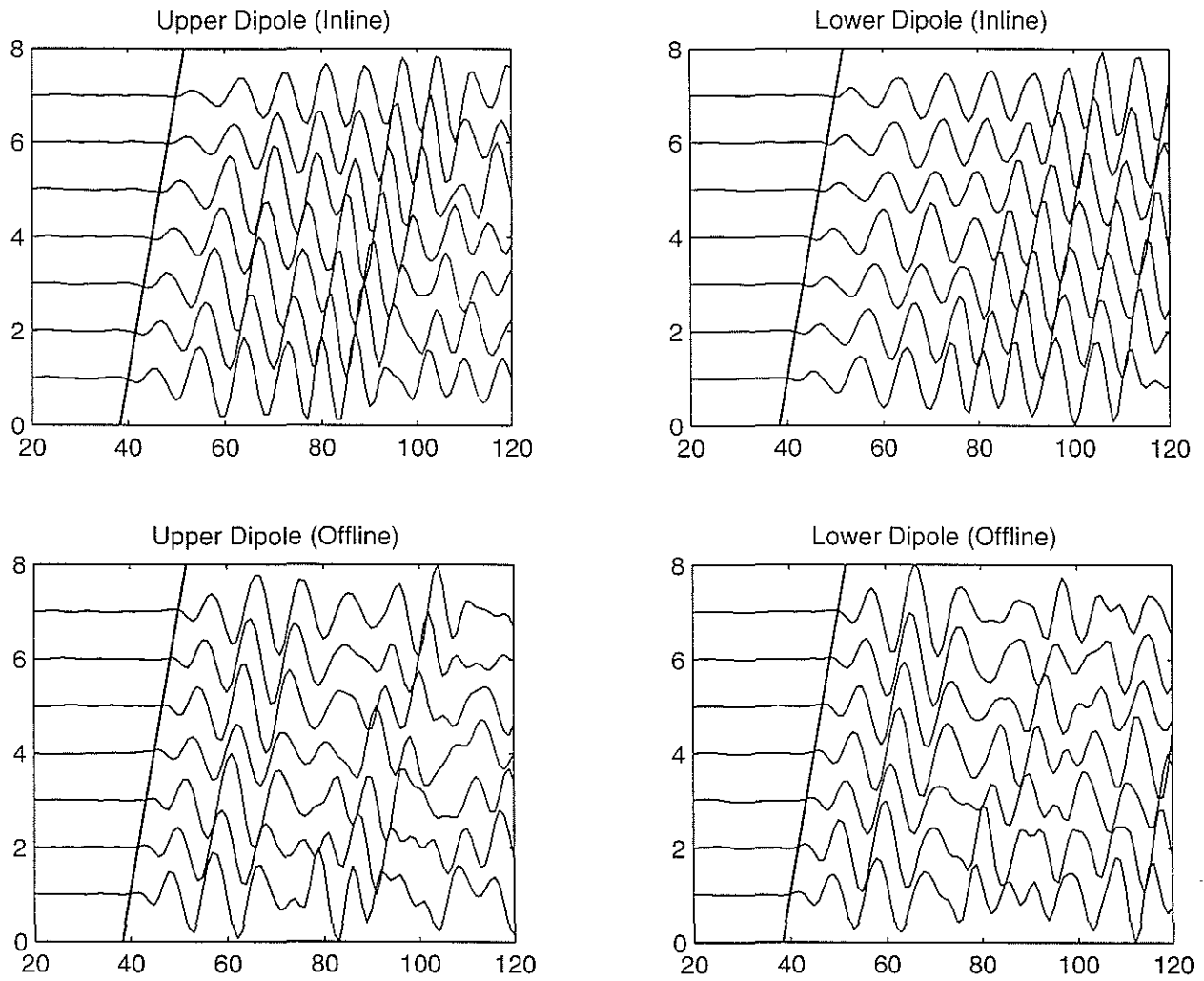
Figure 12: Inline (top 2 pictures) and offline (bottom 2 pictures) components of an anisotropic section. The line in each of the pictures indicates the starting positions of the window used for Alford rotation.
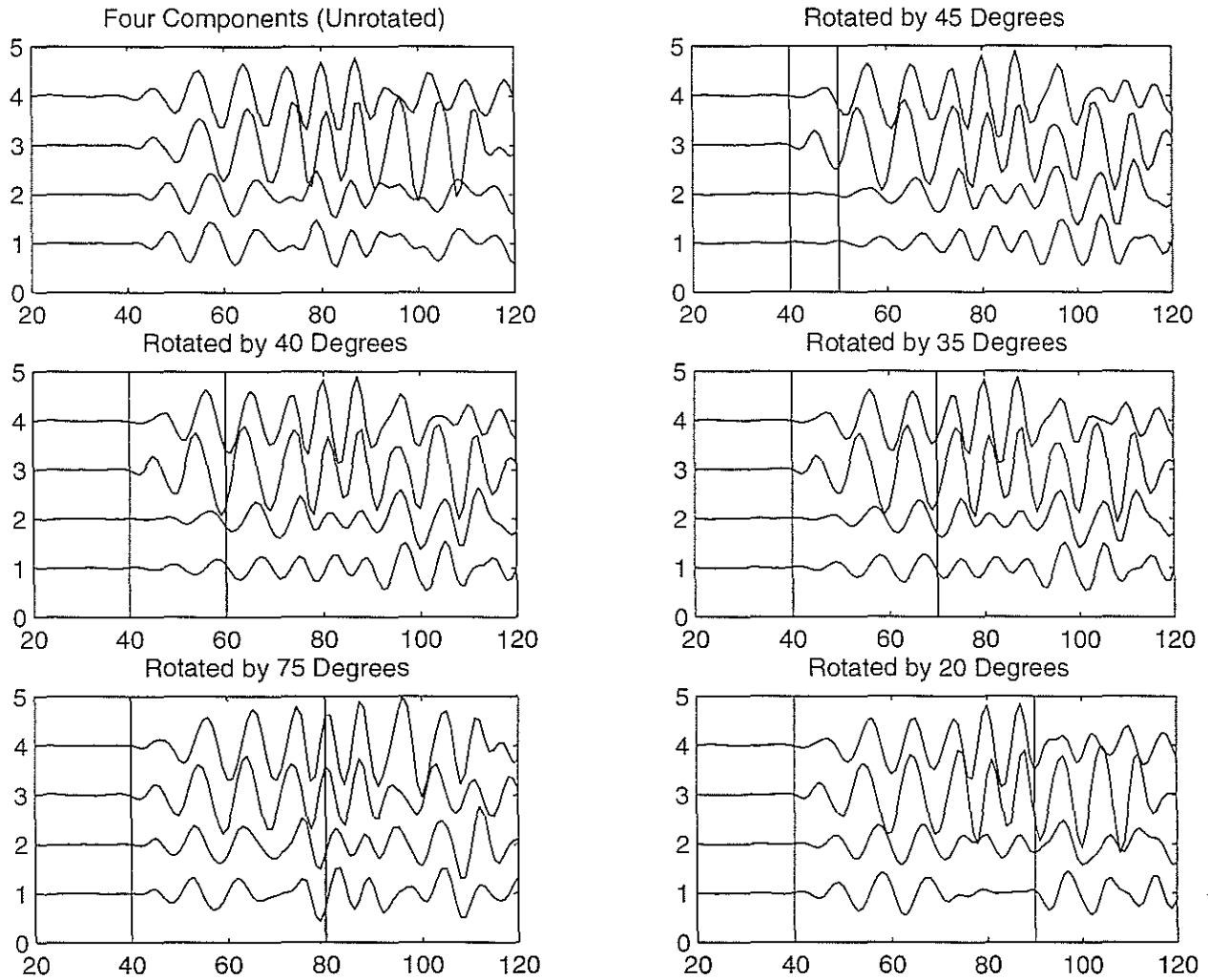
Figure 13: Four components of the first receiver for the unrotated data, and for the data rotated by angles of 45°, 40°, 35°, 75°, and 20°. These angles were determined by minimizing the offline energies in time windows of lengths of 10, 20, 30, 40, and 50 samples, respectively. In each picture the rotation window is indicated by vertical lines.
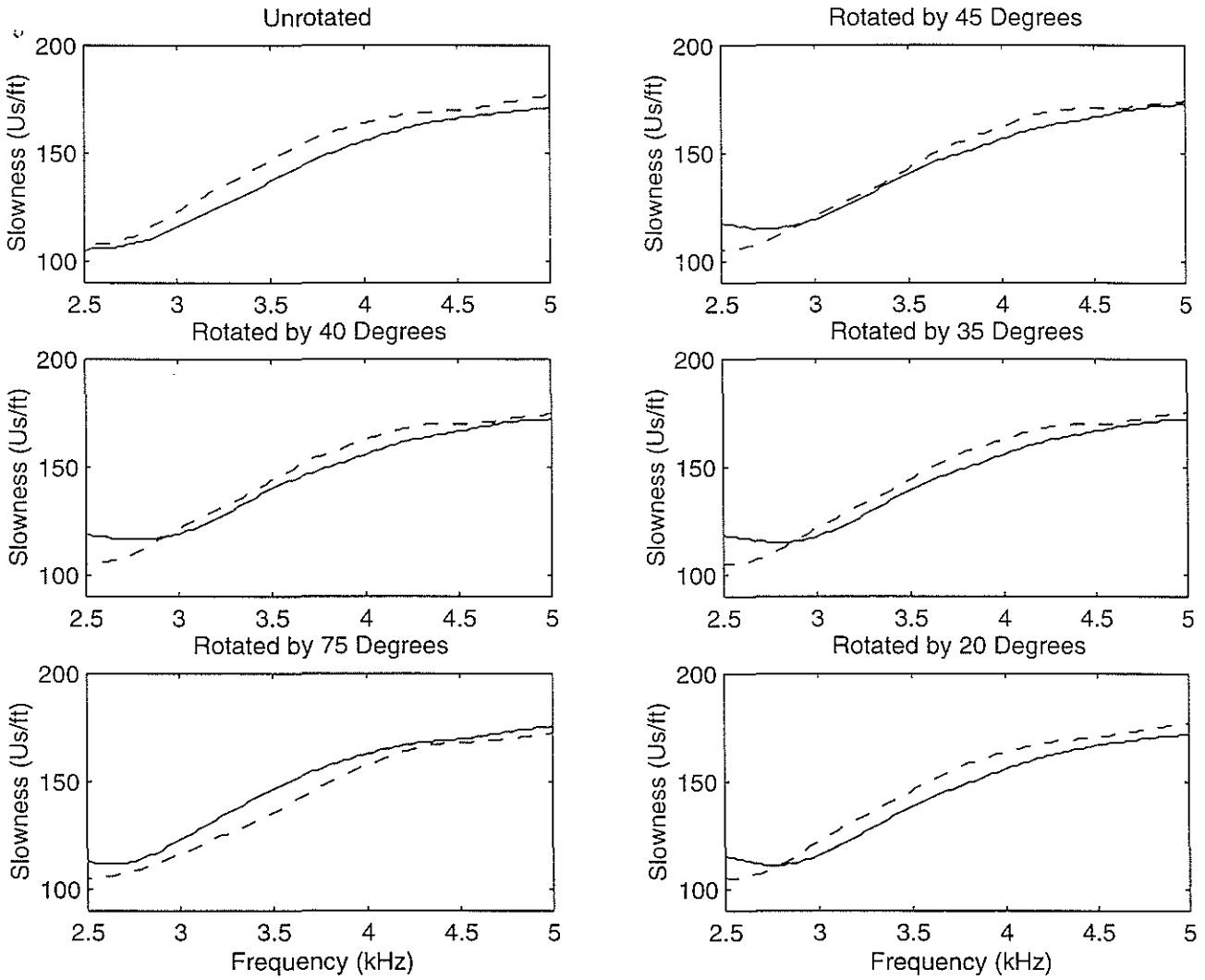
Figure 14: Dispersion curves of the two flexural waves measured on the inline components of the unrotated data and of the data rotated to the angles of Figure 13.